JUL 1 8 1982

431-A-20

TD 4.32/8:80-44

FAA-EE-80-44 R

ORIGINAL

Parameters for Ozone Photolysis as a Function of Temperature at 280-330 NM

Office of Environment
and Energy
Washington, D.C. 20591

COMPLETED
45

John E. Davenport

May 1982

BEST DOCUMENT AVAILABLE

This document is disseminated under the sponsorship of the Department of Transportation in the interest of information exchange. The U.S. Government assumes no liability for its contents or use thereof.

The work reported in this document was conducted under Contract No. DOT-FA78WA-4263 for the Department of Transportation, Federal Aviation Administration. The publication of this report does not indicate endorsement by the Department of Transportation, nor should the contents be construed as reflecting the official position of that agency.

BEST DOCUMENT AVAILABLE

Technical Report Documentation Page

1. Report No.	2. Government Accession No.	3. Recipient's Catalog No.
FAA-EE-80-44 Revised		

4. Title and Subtitle
PARAMETERS FOR OZONE PHOTOLYSIS AS A FUNCTION OF TEMPERATURE AT 280-330 nm

5. Report Date
April 1980 - Revised 1982

6. Performing Organization Code

8. Performing Organization Report No.

7. Author(s)
John E. Davenport

9. Performing Organization Name and Address
SRI International
333 Ravenswood Avenue
Menlo Park, California 94025

10. Work Unit No. (TRAIS)

11. Contract or Grant No.
DOT-FA78WA-4263

12. Sponsoring Agency Name and Address
U.S. Department of Transportation
Federal Aviation Administration
High Altitude Pollution Program
Washington, D.C. 20591

13. Type of Report and Period Covered
Final Report
September 1978 - March 1980

14. Sponsoring Agency Code

15. Supplementary Notes

16. Abstract

This study was undertaken to obtain the parameters for ozone photolysis in the 280-330 nm region as a function of temperature in the 200-300 K range.

The absolute absorption coefficients for O_3 were measured at 298, 271, 225, and 206 K and were tabulated at 1-nm intervals over the 250-370 nm wavelength range. Uncertainties in the absorption coefficients range from 2% at room temperature to about 14% at 206 K and mainly fall in the 3-7% range. Pressure of 0.02-100 torr ozone were used, and no pressure effect was observed up to 800 torr N_2.

The relative $O(^1D)$ quantum yield resulting from laser pulse photolysis of ozone was measured at 300, 260, and 198 K, in the 280-310 nm region by direct observation of the $O(^1D)$ fluorescence at 630 nm. This was the first measurement of the $O(^1D)$ quantum yields based on direct observation of $O(^1D)$ emission. These measurements were put on an absolute basis by measuring the primary quantum yield of $O(^3P)$ at the same temperatures using the $O(^3P)$ resonance fluorescence triplet at 310 nm. This was accomplished by examining the time behavior of the $O(^3P)$ signal in the presence of an excess of N_2, and in the presence of ozone alone.

In general, we found that the time dependence for both $O(^3P)$ and $O(^1D)$ signals were as expected from rate constants in the literature. At room temperature we found about 5 ± 2% $O(^3P)$ formation at 290 nm, and 8 ± 3% at 270 nm.

The implications of the data concerning the detailed photolysis mechanism of ozone and the atmospheric modeling of this process are discussed.

17. Key Words	18. Distribution Statement
Ozone, O_3, Photolysis, Absorption coefficients, Quantum yields, Modeling, Stratosphere.	This document is available to the public through the National Technical Information Service, Springfield, Virginia 22161.

19. Security Classif. (of this report)	20. Security Classif. (of this page)	21. No. of Pages	22. Price
UNCLASSIFIED	UNCLASSIFIED	40	

BEST DOCUMENT AVAILABLE

ABSTRACT

This study was undertaken to obtain the parameters for ozone photolysis in the 280-330 nm region as a function of temperature in the 200-300 K range.

The absolute absorption coefficients for O_3 were measured at 298, 271, 225, and 206 K and were tabulated at 1-nm intervals over the 250-370 nm wavelength range. Uncertainties in the absorption coefficients range from 2% at room temperature to about 14% at 206 K and mainly fall in the 3-7% range. Pressure of 0.02-100 torr ozone were used, and no pressure effect was observed up to 800 torr N_2.

The relative $O(^1D)$ quantum yield resulting from laser pulse photolysis of ozone was measured at 300, 260, and 198 K, in the 280-310 nm region by direct observation of the $O(^1D)$ fluorescence at 630 nm. This was the first measurement of the $O(^1D)$ quantum yields based on direct observation of $O(^1D)$ emission. These measurements were put on an absolute basis by measuring the primary quantum yield of $O(^3P)$ at the same temperatures using the $O(^3P)$ resonance fluorescence triplet at 130 nm. This was accomplished by examining the time behavior of the $O(^3P)$ signal in the presence of an excess of N_2, and in the presence of ozone alone, after it was reconfirmed that $O(^1D) + O_3$ yielded one $O(^3P)$.

In general, we found that the time dependence for both $O(^3P)$ and $O(^1D)$ signals were as expected from rate constants in the literature. At room temperature we found about 5 ± 2% $O(^3P)$ formation at 290 nm, and 8 ± 3% at 270 nm.

The implications of the data concerning the detailed photolysis mechanism of ozone and the atmospheric modeling of this process are discussed.

BEST DOCUMENT AVAILABLE

CONTENTS

ABSTRACT i

ILLUSTRATIONS AND TABLES iii

I INTRODUCTION 1

II OBJECTIVE 4

III ABSORPTION COEFFICIENT MEASUREMENTS 6

A. Details of Apparatus 6

B. Procedures 10

C. Results 11

IV QUANTUM YIELD MEASUREMENTS 18

A. Equipment and Procedures 18

B. Results 21

V DISCUSSION 27a

VI REFERENCES 32

BEST DOCUMENT AVAILABLE

ILLUSTRATIONS

1. Apparatus Used for Making Absorption Coefficient Measurements 7

2. Typical Scan of Ozone Spectrum 14

3. Apparatus Used for Making Quantum Yield Measurements ... 19

4. Typical $O(^1D)$ Emmission Signal 23

5. Room Temperature Values for Atomic Oxygen Quantum Yields 25

TABLES

1. Summary of $O(^1D)$ Quantum Yields at 313 nm 5

2. Summary of Conditions for Absorption Spectrum Measurements 12

3. Absolute Absorption Cross-Sections for Ozone at 253-330 nm from 206-298 K 15

4. Temperature Dependence of Quantum Yields 27

5. Comparison of Absolute Absorption Coefficient Measurements 28

BEST DOCUMENT AVAILABLE

ACKNOWLEDGMENTS

The assistance of Bosco Lan in the construction of apparatus is hereby acknowledged. Dr. Dale Hendry, Dr. Tom Slanger and Dr. Graham Black, along with the use of some of their equipment, were helpful in resolving several experimental difficulties, and conversations with them helped develop a clearer picture of the ozone photolysis mechanism in the UV region. Dr. Ted Mill has also assisted in this project by reviewing reports and acting as project supervisor.

BEST DOCUMENT AVAILABLE

I INTRODUCTION

The biological role of atmospheric ozone as an ultraviolet (UV) shield and as a pollutant in the urban troposphere make it important to obtain accurate ozone kinetics and photolysis parameters. Ozone photolysis is the main process by which UV radiation from the sun is converted into thermal energy in the daytime stratosphere, and thus it plays an important role in the energy cycle of the earth. The UV photolysis of ozone is the dominant daytime production process for O-atoms within the stratosphere, and along with the recombination process, it determines the daytime O-atom concentration in the middle and lower stratosphere. Johnston[1] has noted that calculations based on the simple Chapman mechanism

$$O_2 + h\nu \rightarrow O + O \quad (1)$$

$$O + O + M \rightarrow O_2 + M \quad (2)$$

$$O + O_2 + M \rightarrow O_3 + M \quad (3)$$

$$O_3 + h\nu \rightarrow O + O_2 \quad (4)$$

$$O + O_3 \rightarrow 2O_2 \quad (5)$$

lead to calculated ozone concentrations that are too large by a factor of 5. He has suggested that trace constitutents, most notably NO and NO_2, destroy ozone, beginning with ozone photolysis to produce $O(^1D)$ followed by:

$$O(^1D) + N_2O \rightarrow 2NO \quad \text{(as well as } N_2 + O_2) \quad (6)$$

Then, the NO formed in reaction (6) is available to catalyze the destruction of O_3 and O:

$$NO + O_3 \rightarrow NO_2 + O_2 \quad (7)$$

$$\underline{O + NO_2 \rightarrow NO + O_2} \quad (8)$$

$$\text{Net:} \quad O_3 + O \rightarrow O + 2O_2$$

In addition to this NO/NO_2 cycle, the H/OH cycle also destroys odd-oxygen species and is mainly initiated by $O(^1D)$ reaction with atmospheric

BEST DOCUMENT AVAILABLE

water vapor. The sequence of reactions is initiated by

$$O(^1D) + H_2O \rightarrow 2OH \qquad (9)$$

followed by the catalytic cycle:

$$OH + O \rightarrow O_2 \qquad (10)$$

$$\underline{H + O_3 \rightarrow O_2} \qquad (11)$$

$$\text{Net:} \quad O + O_3 \rightarrow 2O_2 \qquad (10) + (11)$$

A similar odd-oxygen destruction also occurs in a Cl/ClO cycle, although in this case the main initiating step is photolysis of the Cl-containing molecule rather than reaction with $O(^1D)$ from ozone photolysis.

Thus, because of the dominant role played by $O(^1D)$ reactions in initiating two catalytic cycles that destroy odd-oxygen species (mainly O and O_3), it is important to know the rate of production of $O(^1D)$ in the stratosphere; this rate is controlled by the rate of ozone photolysis in the Hartley band. To calculate this rate, we must know the absorption spectrum and quantum yield accurately as a function of temperature.

Literature values for the absorption cross sections[2,13] are in good agreement in the Hartley band (200-310 nm) at room temperature. Previous to the current study, however, Vigroux[5,11] completed the only studies of ozone absorption coefficient dependence on temperature in the spectral region between 245 and 345 nm. He found that the absorption cross section was reduced most with lowering temperature at wavelengths that corresponded to minima in the Huggins band intensities (as at 329.9 nm, for instance) and therefore to high rotational numbers. He also found that the effect of temperature changes was greater at long wavelengths than at short ones. He concluded that the effect of reducing temperature was not due as much to the shifting of the onset of $O(^1D)$ production as to the reduction in ground-state ozone internal energy.

In the Huggins region,[14,22] a quantum yield of one for the process:

$$O_3 + h\nu \rightarrow O_2(^1\Delta) + O(^3P) \qquad (12)$$

seems to be firmly established at wavelengths greater than 320 nm; this is based on total ozone disappearance quantum yields of 4.0, independent of temperature, and on spectroscopic observations[15,23] of the $O_2(^1\Delta)$ emission,

BEST DOCUMENT AVAILABLE

which is proportional to the O_3 photolysis rate and is independent of N_2 or O_2 pressures.

The atmospherically important photolysis process takes place in the Hartley band, with the near unit quantum efficiency[21,24,25]:

$$O_3 + h\nu \rightarrow O_2(^1\Delta) + O(^1D) \qquad (13)$$

Many studies have been made near the 308 nm $O(^1D)$ cut-off region. No absolute quantum yield measurements exist for $O(^1D)$ production, $\phi(^1D)$, for this whole region, and quantum yields at 313 nm (see Table 1) show values ranging from less than 0.1 to 1.0. Most of these studies assumed unit quantum yield for $O(^1D)$ production at the quantum yield plateau at $\lambda \leq 308$ nm. Recently, however, Fairchild et al.[34] obtained results implying that the $O(^1D)$ quantum yield varies significantly in the wavelength region around the cut-off. They found a monotonic decrease in $O(^1D)$ quantum yields as the wavelength decreased below 308 nm. They measured a value for $\phi(^1D)$ of 0.87 at 274 nm. In retrospect, the data of Lin and Demore,[31] which they normalized at an $O(^1D)$ quantum yield of 1.0 at 300 nm, also shows a drop-off in the quantum yield of isobutanol formation at shorter wavelengths; this drop-off was barely perceptible given their experimental uncertainty. Recently Wiesenfeld[35] and also Sparks et al.[36] have reported results coinciding with Lawrence's observation. However, earlier work by Wiesenfeld,[37] using the same methods as in the recent study,[35] gave a value of $\phi(^3P)$ of zero at 266 nm. E. K. Lee[38] only found $\phi(^1D)$ decrease with increasing wavelength as the cutoff is approached in contrast to other workers.

To summarize, then, the temperature dependence of the absorption coefficients has been tabulated only once for wavelengths above 254 nm. The quantum yields for product paths at long wavelengths seem well established and acceptable from the viewpoint of stratospheric and tropospheric modeling. However, the quantum yields for $O(^1D)$ production in the Harley band show much disagreement, especially in the critical 300-320 nm region. In any case, none were based on absolute measurement of the $O(^3P)$ and $O(^1D)$ species produced at least not until after this study was undertaken.

BEST DOCUMENT AVAILABLE

II OBJECTIVE

The objective of this work was to obtain accurate and precise quantum yields and absorption coefficients for ozone photolysis in the 280-330 nm region for atmospheric modeling purposes. Specifically, our method of approach had several advantages over previous systems designed to achieve this objective:

- A long path, temperature-controlled cell was used to obtain quantum yields, making it possible to measure the very low $\phi(^1D)$ values in the Huggins band.
- The absorption data are tabulated for modeling purposes.
- For the first time, direct observation of $O(^1D)$ formed the basis for the relative quantum yield measurements. Thus, the solvent effects and the effects of temperature on secondary reactions cannot cause systematic errors.
- We also measured absolute $O(^3P)$ quantum yields by direct observation of $O(^3P)$. This overcome the problems encountered in previous efforts, which for the most part entailed arbitrary normalization to unity at 300 nm.
- Because primary $O(^3P)$ quantum yields, $\phi(^3P)$, are relatively small in the Hartley Band, and since production of stable excited O_3 does not occur, small uncertainties in $O(^3P)$ production leads to extremely precise values of $\phi(^1D)$. That is, since $\phi(^3P)$, $\phi(^1D)$, and the uncertainties in the quantum yields $\Delta\phi(^1D)$ and $\Delta\phi(^3P)$ are related by:

$$\frac{\Delta\phi(^1D)}{\phi(^1D)} = \frac{\Delta\phi(^3P)}{1 - \phi(^3P)} \qquad (14)$$

For the relatively small values of $\phi(^3P)$ and even smaller uncertainties, the precision in the derived $O(^1D)$ quantum yields are much better than can be obtained by measuring $\phi(^1D)$ directly with the same relative precision.

BEST DOCUMENT AVAILABLE

Table 1

SUMMARY OF $O(^1D)$ QUANTUM YIELDS AT 313 nm

Investigators	$\phi O(^1D)$	Temperature (K)	Technique	Photolytic Source
Castellano and Schumacher (Ref. 20)	1.0	298	Gas phase O_3; decrease in O_2 pressure	cw lamp
Kajimoto and Cvetanovic (Ref. 26)	0.53 0.21	313 298	Gas phase O_3; N_2O; increase in N_2	cw lamp chemical filter
Martin, Girman, and Johnston (Ref. 27)	0.32	298	O_3, N_2O; chemiluminescence	cw lamp
Moortgatt and Warneck (Ref. 28)	0.29	298	O_3, N_2O; NO_2 chemiluminescence	cw lamp
Kuis, Simonaitis, and Heicklen (Ref. 29)	0.29 0.22 0.11	293 258 221	Gas phase O_3, O_2, N_2O; increase in N_2	cw lamp chemical filter
Jones and Wayne (Ref. 30)	0.1	298	Decrease in O_3	cw lamp
Lin and DeMore (Ref. 31)	0.08	235	O_3, isobutane	cw lamp
Philen, Watson, and Davis (Ref. 32)	0.12	298	O_3, N_2O, NO_2 chemiluminescence	Pulsed dye laser
Arnold, Comes, and Moortgatt (Ref. 33)	0.20	298	Gas phase O_3, N_2O, NO_2 chemiluminescence	Pulsed dye laser
This work	0.19 ± 0.09 0.15 ± 0.13 0.04 ± 0.10	300 268 198	Gas phase O_3, $O(^1D)$ emission $O(^3P)$ resonance fluorescence	Pulsed dye laser

BEST DOCUMENT AVAILABLE

III ABSORPTION COEFFICIENT MEASUREMENTS

A. Details of Apparatus

The basic apparatus used to measure the ozone absorption coefficients is shown schematically in Figure 1. It consisted of a light source; a regulated lamp power supply and monitoring system; a gas purification, mixing and pumping system; a Perkin Elmer "40-meter" multiple-reflection White cell; an ethylene glycol cooling and circulation system; and an MPI 1018B monochromator with 1P28 photomultiplier; and a picoammeter and recorder.

Three light sources were actually used. The main light source, used primarily in the 250-300 nm region, was a Hanovia 795C-394 2500 watt, high-pressure xenon lamp. It was housed in Oriel Model 6153 Universal lamp housing with 100-mm quartz optics. The regulated power supply was adjusted to provide 2000 watts for all experiments. After an initial warm-up period of about 10 minutes, the observed intensity did not change more than 1% in any one period of up to 8 hours continuous use. The light was passed through a 10-cm water-cooled water filter to eliminate IR radiation. Corning glass filters 7-54 and 7-59 were used both at the entrance to the cell and just behind the entrance slit of the monochromator. These filters were used to minimize the amount of scattered light and thus reduce the wavelength dependence of the background to an immeasurably small value. All these filters helped to protect the optical surfaces and slits in the system from high intensity UV radiation and heat damage. In principle, the Hanovia lamp was the most useful point source because it was continuous over the whole range and because it was very intense, which allowed us to use narrow slit widths (limited only by the monochromator geometry). However, its disadvantages, mainly its fragility and the unreliability in its supply, led us to use a hydrogen continuum source in the 290-330 nm region. The lamp was from a Beckman DU spectrophotometer. It is smoothly continuous and the output spectrum is relatively flat in the 290-330 nm region. Below about 290 nm, the

BEST DOCUMENT AVAILABLE

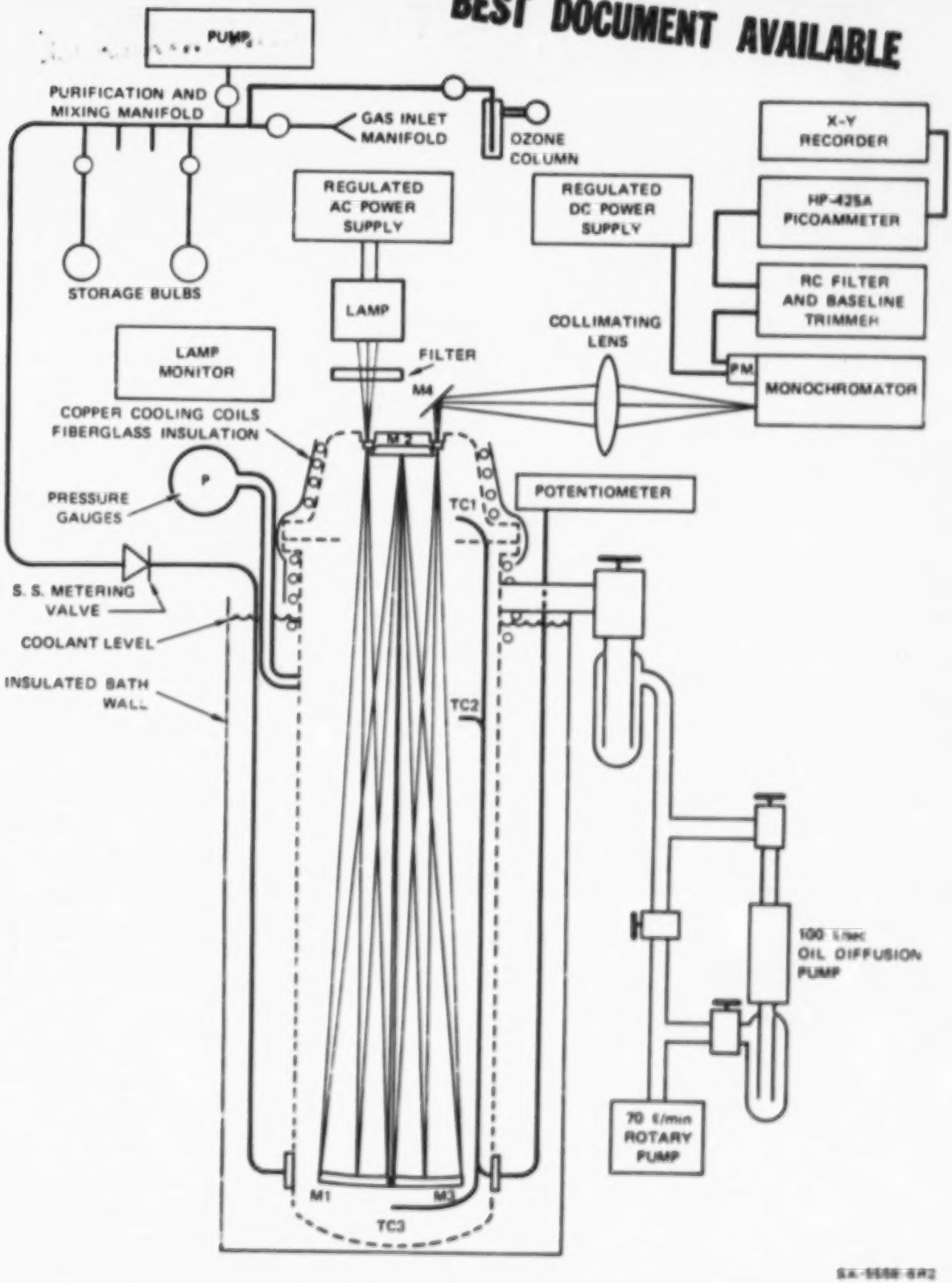

FIGURE 1 APPARATUS USED IN MAKING ABSORPTION COEFFICIENT MEASUREMENTS

Shown for use in taking absorption data taken over 308-cm path length. M1, 2, 3, 4, are system mirrors in order of light incidence. TC 1, 2, 3, represent thermocouple leads.

BEST DOCUMENT AVAILABLE

intensity drops off rather quickly. Above about 350 nm, the emission spectrum becomes too structured to be useful. Thus, a tungsten filament, incandescent quartz halogen lamp was used in the 350-370 region.

The gas-handling system consiste of three parts: a stainless steel gas inlet system, a glass storage system with Teflon stopcocks, and a copper and rubber tube exhaust pumping system. Pressures were measured with a Texas Instruments (TI) Bourden cell gauge for most experiments down to one torr; a transducer was used at pressures down to 10 millitorr. Both systems were standardized against a McLeod gauge. The TI gauge had an uncertainty of less than ± 10 millitorr at all pressures used, and the transducer precision was about ± 1%.

A Perkin-Elmer multiple-reflection White cell, with 15-cm main optics, was used as the absorption cell. The mirrors were aluminum-coated with a thin SiO_2 overcoat that is inert to the ozone at the high pressures present during some of these experiments. The maximum path length was limited to 32 m by the combination of surface reflectance, light intensity, and detector sensitivity. The total path lengths in the cooled Perkin-Elmer system were measured to within 1% by direct measurement. This uncertainty includes the slight difference in path lengths for light striking the edges and the center of the mirrors. Inlet and outlet apertures were 5-mm wide; the sealing gaskets were made of Viton.

The reaction cell was placed in a 50-gallon insulated cooling bath, deep enough to immerse about 85% of the cell. The other 15%, with the input optics was cooled with coils through which the bath liquid was circulated. At -67°C it was found convenient to pack the top with dry ice to maintain the internal temperature.

Cooling bath equipment also included a 60-gal/min circulation pump, a 500-ml/min parastalic pump for the cooling coils, and a cooling bath capable of cooling the system to 273 K overnight without using dry ice or liquid nitrogen. The coolant selected was 70% ethylene glycol in water. This mixture remained liquid down to around 198 K, measured by alcohol thermometer outside the photolysis cell. Temperatures inside the cell were measured using three thermocouples: one at the bottom of

BEST DOCUMENT AVAILABLE

the cell, one at about the liquid level, and one at the uppermost portion of the cell.

The light from the lamp passed directly into the entrance aperture through a 6-mm quartz-plate window, traveled through the multiple reflection path, and passed back out through another 6-mm quartz-plate window of the exit aperture. Dry nitrogen was passed over both windows to prevent condensation of atmospheric moisture. After exiting the cell, the light was reflected by a plane mirror through a quartz condensing lens, which focused it on the slit of the MP-1018D 0.45-meter scanning monochromator. The grating used in these experiments was a 2360-groove/mm Jarrell-Ash replica grating blazed for maximum intensity at 270 nm in first order.

A 1P28 photomultiplier detection system--including a high voltage DC power supply, a Keithley Model 480 digital picoammeter, and a strip-chart recorder--was used to measure the intensity of the emerging light beam. The wavelength resolution of the system using 10-μm slits reduced to 1 mm in height was better than 0.037 nm, based on measuring the full width at half maximum of the 253.67-nm line from a low-pressure mercury source.

The ozone was produced using a Wellsbach Model T-408 silent discharge ozone generator, which delivers up to 4% O_3 in an atmosphere of O_2 at a flow rate as high as 4.0 liters/min. This mixture was passed through a silica gel column that preferentially adsorbed the ozone. When the column was loaded with the maximum amount of ozone at -78°C, the ozone generator was turned off and the column was isolated from it and the exhaust system. Next, the valve to the rotary pump, which was protected by a rubber tubing inlet, was opened. The column was pumped down to less than 200 millitorr pressure at -78°C. To obtain the pure ozone, the dry ice bath was removed and the pressure of the ozone was allowed to increase in the absorption cell to as high as 50 torr. The ozone decomposes very slowly on these columns so that pumping down is necessary about one time per day to remove the oxygen formed.

BEST DOCUMENT AVAILABLE

In the aluminum absorption cell, the rate of photolysis of the ozone was negligibly and unmeasurably small. However, wall decomposition rates were too high initially (30 min half-life) and were reduced by leaving about 50 torr ozone in the cell overnight for several nights, for a total cell conditioning time of about 48 hours. No leaks were produced by this method and the ozone decomposed at a rate of less than 10% per hour at first, and after many months of experiments, it decomposed at a rate of less than 2% per hour. Thus, ozone pressure measurement accuracy was limited only by the initial uncertainty in the oxygen purity and in the pressure measuring apparatus.

B. Procedures

The procedures were essentially the same at all temperatures. After the reaction cell was pumped down to less than 10^{-4}, the system linearity was checked, as well as the O_3 destruction rate in the cell. This was accomplished by first measuring the absorption as a function of pressure at a monochromator setting of 300 nm, which was actually 299.71 nm. A flowing system was used to take these intensity measurements as the pressure was increased in increments. Then the system was pumped out in increments, resulting in I_o/I static measurements at the same pressures as used in the flowing system measurements. The plot of log I_o/I as a function of total pressure established the linearity of the measured photocurrent with transmitted intensity. In addition, there was no significant difference between the absorption measurements for a flowing system and the static system, which indicated that any unexpected pressure gradients would not affect measurements done in a flow system mode, and that significant destruction of O_3 did not occur in the static measurements. This check was performed at each temperature, and in each case a static system could be used to obtain precise and linear data.

Several runs were made over the same region with at least three different electronic filtering time constants ranging up to 2 seconds to be sure that no spurious peaks appeared and no absorption features were

BEST DOCUMENT AVAILABLE

obliterated. A lamp monitor was used to be sure the lamp intensity did not vary more than 1% during each run. However, because of drift in the electronics, it was necessary to reset initial conditions and begin a retrace. If there was more than 0.5% shift in the measured intensity, the run was not used and the scan was repeated.

The spectra were measured in overlapping 5-20 nm sections. The length of a section was determined by the variations in both the continuum intensities and the absorption intensities. In the 280-300 nm region the intensity gradients were so large that the ozone pressure had to be adjusted every 5 nm to meet the twin requirements of having enough photocurrent to measure accurately and yet not go off scale, since an error was introduced when the picoammeter scales were changed during a run.

A typical scan would begin by pumping down the cell and obtaining an initial background intensity spectrum. Ozone was then added to the desired pressure, and an absorption scan was taken. These survey scans were used to establish the overall relations of the parameters involved and was to establish reference volumes for absorption coefficients. Better values for reactive absorbance were obtained from data such as that in Figure 2 where the vertical scale is expanded. These scans were the ones used to determine the absorption cross sections at 1 nm intervals at wavelengths determined by calibrating the monochromator using a low pressure mercury lamp.

C. Results

Table 2 summarizes the experimental conditions for the absorption coefficient measurements. Figure 2 shows a sample from an interesting part of the spectrum as discussed later. The values obtained for the extinction coefficients were calculated from:

$$\sigma = \frac{\ln(I_o/I)}{\ell\beta P_{O_3}}\left(\frac{298}{T}\right) \qquad (15)$$

and are shown in Table 3. In equation (15), I_o is the relative lamp intensity at a given wavelength, I is the transmitted intensity at the

Table 2

SUMMARY OF CONDITIONS FOR ABSORPTION SPECTRUM MEASUREMENTS

	Wavelength Range 250-300	Wavelength Range 290-330	Wavelength Range 330-370
Lamp Used	Xenon	Xenon and hydrogen	Incandescent
Ozone Pressure (torr)	0.1-1	1-50	10-100
Pressure After Nitrogen Addition (torr)	810	780	760
Slit Width (μm)	10-40	10-40	10-50
Band Pass (nm)	0.06-0.24	0.06-0.24	.06-0.30
Estimated Precision of I/I_o from 330 to 370 nm	± 5%	± 3%	Greater of
from 300 to nm	± 3%		$\pm 1 \times 10^{-24}$ cm^{-2}
			± 5%

BEST DOCUMENT AVAILABLE

BEST DOCUMENT AVAILABLE

same wavelength, ℓ is the path length, P_{O_3} is the pressure of ozone in torr, and β is a consant that relates pressure to concentration at 298 K: 3.24×10^{16} molec-sec^{-1} per torr.

BEST DOCUMENT AVAILABLE

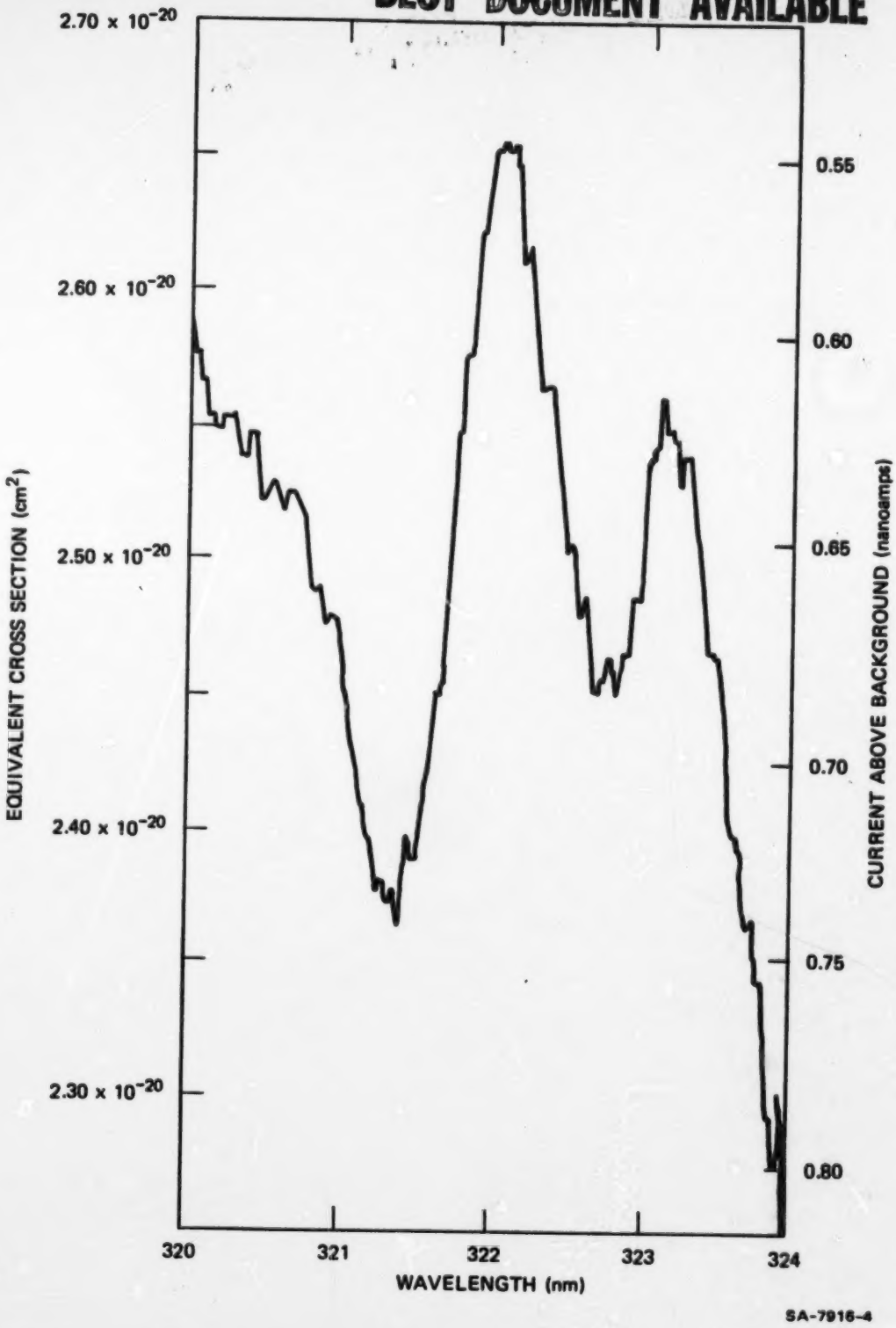

FIGURE 2 TYPICAL SCAN OF OZONE SPECTRUM

Expanded scale spectrum of 320-324 nm region. 17.3 torr ozone, 398 cm path length, 10 μm slit width. Half width resolution: 0.04 nm. Scan speed 1.0 nm/min. Light source: high pressure hydrogen lamp. 700 Volts on 1P28 photomultiplier.

BEST DOCUMENT AVAILABLE

Table 3

ABSOLUTE ABSORPTION CROSS-SECTIONS FOR OZONE
AT 253-330 nm from 206-298K

Wavelength (nm)	298K	271K	225K	206K
253	1.21×10^{-17}	1.10×10^{-17}	1.08×10^{-17}	1.09×10^{-17}
254	1.41×10^{-17}	1.37×10^{-17}	1.33×10^{-17}	1.31×10^{-17}
255	1.15×10^{-17}	1.06×10^{-17}	1.09×10^{-17}	1.08×10^{-17}
256	1.32×10^{-17}	1.34×10^{-17}	1.31×10^{-17}	1.29×10^{-17}
257	9.71×10^{-18}	9.90×10^{-18}	9.61×10^{-18}	9.60×10^{-18}
258	1.11×10^{-17}	1.11×10^{-17}	1.08×10^{-17}	1.02×10^{-17}
259	1.13×10^{-17}	1.10×10^{-17}	1.09×10^{-17}	1.07×10^{-17}
260	1.14×10^{-17}	1.11×10^{-17}	1.08×10^{-17}	1.04×10^{-17}
261	1.08×10^{-17}	1.05×10^{-17}	1.01×10^{-17}	1.00×10^{-17}
262	1.05×10^{-17}	1.06×10^{-17}	1.00×10^{-17}	9.68×10^{-18}
263	1.03×10^{-17}	9.98×10^{-18}	9.38×10^{-18}	9.31×10^{-18}
264	1.03×10^{-17}	9.81×10^{-18}	9.42×10^{-18}	9.26×10^{-18}
265	9.67×10^{-18}	9.29×10^{-18}	9.11×10^{-18}	9.10×10^{-18}
266	9.10×10^{-18}	9.07×10^{-18}	9.05×10^{-18}	9.06×10^{-18}
267	8.7×10^{-18}	8.54×10^{-18}	8.49×10^{-18}	8.39×10^{-18}
268	7.57×10^{-18}	8.18×10^{-18}	8.07×10^{-18}	8.02×10^{-18}
269	8.24×10^{-18}	7.85×10^{-18}	7.81×10^{-18}	7.79×10^{-18}
270	7.81×10^{-18}	7.76×10^{-18}	7.61×10^{-18}	7.58×10^{-18}
271	7.82×10^{-18}	7.26×10^{-18}	7.20×10^{-18}	7.21×10^{-18}
272	6.95×10^{-18}	6.91×10^{-18}	6.90×10^{-18}	6.83×10^{-18}
273	6.24×10^{-18}	6.30×10^{-18}	6.21×10^{-18}	6.12×10^{-18}
274	5.82×10^{-18}	5.85×10^{-18}	5.51×10^{-18}	5.43×10^{-18}
275	5.51×10^{-18}	5.31×10^{-18}	5.20×10^{-18}	5.13×10^{-18}
276	5.16×10^{-18}	5.17×10^{-18}	5.13×10^{-18}	5.01×10^{-18}
277	5.03×10^{-18}	4.84×10^{-18}	4.80×10^{-18}	4.71×10^{-18}
278	4.58×10^{-18}	4.42×10^{-18}	4.31×10^{-18}	4.30×10^{-18}
279	4.04×10^{-18}	4.08×10^{-18}	4.01×10^{-18}	3.99×10^{-18}
280	3.85×10^{-18}	3.81×10^{-18}	3.81×10^{-18}	3.78×10^{-18}
281	3.45×10^{-18}	3.46×10^{-18}	3.39×10^{-18}	3.40×10^{-18}
282	3.40×10^{-18}	3.20×10^{-18}	3.21×10^{-18}	3.16×10^{-18}
283	3.04×10^{-18}	3.00×10^{-18}	3.01×10^{-18}	2.94×10^{-18}
284	2.66×10^{-18}	2.61×10^{-18}	2.55×10^{-18}	2.56×10^{-18}
285	2.42×10^{-18}	2.34×10^{-18}	2.31×10^{-18}	2.30×10^{-18}
286	2.07×10^{-18}	2.19×10^{-18}	2.02×10^{-18}	1.98×10^{-18}
287	2.00×10^{-18}	1.94×10^{-18}	1.92×10^{-18}	1.90×10^{-18}
288	1.70×10^{-18}	1.51×10^{-18}	1.48×10^{-18}	1.46×10^{-18}
289	1.54×10^{-18}	1.50×10^{-18}	1.41×10^{-18}	1.40×10^{-18}
290	1.35×10^{-18}	1.31×10^{-18}	1.21×10^{-18}	1.20×10^{-18}
291	1.21×10^{-18}	1.91×10^{-18}	1.00×10^{-18}	9.98×10^{-19}
292	1.10×10^{-18}	1.05×10^{-18}	1.01×10^{-18}	9.99×10^{-19}
293	8.39×10^{-19}	8.96×10^{-19}	8.45×10^{-19}	8.20×10^{-19}
294	8.31×10^{-19}	8.30×10^{-19}	8.29×10^{-19}	8.21×10^{-19}
295	7.88×10^{-19}	7.79×10^{-19}	7.71×10^{-19}	7.70×10^{-19}

Cross-sections in cm^2.

BEST DOCUMENT AVAILABLE

Table 3 (Continued)

Wavelength (nm)	298K	271K	225K	206K
296	6.47×10^{-19}	6.40×10^{-19}	6.40×10^{-19}	6.38×10^{-19}
297	5.77×10^{-19}	5.70×10^{-19}	5.64×10^{-19}	5.60×10^{-19}
298	4.45×10^{-19}	4.18×10^{-19}	4.07×10^{-19}	4.04×10^{-19}
299	4.48×10^{-19}	4.15×10^{-19}	4.10×10^{-19}	4.03×10^{-19}
300	4.09×10^{-19}	3.96×10^{-19}	3.90×10^{-19}	3.85×10^{-19}
301	3.49×10^{-19}	3.31×10^{-19}	3.21×10^{-19}	3.20×10^{-19}
302	3.13×10^{-19}	2.96×10^{-19}	2.92×10^{-19}	2.91×10^{-19}
303	2.68×10^{-19}	2.60×10^{-19}	2.51×10^{-19}	2.48×10^{-19}
304	2.15×10^{-19}	2.28×10^{-19}	2.17×10^{-19}	2.08×10^{-19}
305	2.11×10^{-19}	1.99×10^{-19}	1.95×10^{-19}	1.91×10^{-19}
306	1.83×10^{-19}	1.79×10^{-19}	1.75×10^{-19}	1.73×10^{-19}
307	1.61×10^{-19}	1.55×10^{-19}	1.53×10^{-19}	1.49×10^{-19}
308	1.48×10^{-19}	1.51×10^{-19}	1.49×10^{-19}	1.51×10^{-19}
309	1.21×10^{-19}	1.23×10^{-19}	1.19×10^{-19}	1.12×10^{-19}
310	9.92×10^{-20}	9.81×10^{-20}	9.42×10^{-20}	9.89×10^{-20}
311	9.52×10^{-20}	9.48×10^{-20}	9.30×10^{-20}	9.10×10^{-20}
312	8.07×10^{-20}	7.41×10^{-20}	7.25×10^{-20}	6.92×10^{-20}
313	6.93×10^{-20}	6.73×10^{-20}	6.61×10^{-20}	6.54×10^{-20}
314	6.35×10^{-20}	5.14×10^{-20}	4.50×10^{-20}	3.96×10^{-20}
315	5.24×10^{-20}	5.01×10^{-20}	4.62×10^{-20}	4.54×10^{-20}
316	5.16×10^{-20}	4.98×10^{-20}	4.22×10^{-20}	4.19×10^{-20}
317	4.12×10^{-20}	3.83×10^{-20}	3.36×10^{-20}	2.98×10^{-20}
318	3.74×10^{-20}	3.41×10^{-20}	3.21×10^{-20}	2.79×10^{-20}
319	2.80×10^{-20}	2.51×10^{-20}	2.32×10^{-20}	2.11×10^{-20}
320	2.59×10^{-20}	2.49×10^{-20}	2.43×10^{-20}	2.40×10^{-20}
321	2.43×10^{-20}	2.26×10^{-20}	9.91×10^{-21}	8.96×10^{-21}
322	2.65×10^{-20}	2.13×10^{-20}	2.02×10^{-20}	1.98×10^{-20}
323	2.54×10^{-20}	1.92×10^{-20}	1.36×10^{-20}	1.38×10^{-20}
324	2.25×10^{-20}	1.80×10^{-20}	1.53×10^{-20}	1.38×10^{-20}
325	1.84×10^{-20}	1.61×10^{-20}	1.38×10^{-20}	1.04×10^{-20}
326	1.16×10^{-20}	1.11×10^{-20}	9.82×10^{-21}	9.63×10^{-21}
327	9.27×10^{-21}	7.94×10^{-21}	6.03×10^{-21}	5.93×10^{-21}
328	1.31×10^{-20}	1.29×10^{-20}	1.29×10^{-20}	1.30×10^{-20}
329	9.38×10^{-21}	6.86×10^{-21}	5.61×10^{-21}	4.64×10^{-21}
330	6.68×10^{-21}	6.01×10^{-21}	5.03×10^{-21}	4.10×10^{-21}

Cross sections in cm^2.

BEST DOCUMENT AVAILABLE

Table 3 (Concluded)

Wavelength (nm)	298°K	271°K	225°K	206°K
331	7.29×10^{-21}	6.94×10^{-21}	5.80×10^{-21}	5.39×10^{-21}
332	6.97×10^{-21}	4.84×10^{-21}	3.12×10^{-21}	2.50×10^{-21}
333	4.74×10^{-21}	3.63×10^{-21}	2.71×10^{-21}	1.77×10^{-21}
334	5.66×10^{-21}	5.62×10^{-21}	5.61×10^{-21}	5.60×10^{-21}
335	2.53×10^{-21}	2.21×10^{-21}	1.95×10^{-21}	1.60×10^{-21}
336	2.60×10^{-21}	2.11×10^{-21}	1.01×10^{-21}	7.33×10^{-22}
337	3.81×10^{-21}	3.61×10^{-21}	1.82×10^{-21}	1.78×10^{-21}
338	2.57×10^{-21}	2.47×10^{-21}	1.92×10^{-21}	1.33×10^{-21}
339	1.32×10^{-21}	9.84×10^{-22}	6.12×10^{-22}	4.99×10^{-22}
340	2.04×10^{-21}	1.13×10^{-21}	7.26×10^{-22}	6.81×10^{-22}
341	1.01×10^{-21}	8.64×10^{-22}	7.41×10^{-22}	7.30×10^{-22}
342	7.65×10^{-22}	6.21×10^{-22}	3.19×10^{-22}	2.25×10^{-22}
343	9.64×10^{-22}	7.01×10^{-22}	4.29×10^{-22}	1.43×10^{-22}
344	1.24×10^{-21}	1.02×10^{-21}	9.9×10^{-23}	9.0×10^{-23}
345	6.26×10^{-22}	5.74×10^{-22}	4.25×10^{-22}	3.01×10^{-22}
346	5.77×10^{-22}	1.21×10^{-22}	8.4×10^{-23}	5.9×10^{-23}
347	5.22×10^{-22}	5.01×10^{-22}	4.56×10^{-22}	4.49×10^{-22}
348	3.62×10^{-22}	3.64×10^{-22}	3.20×10^{-22}	2.73×10^{-22}
349	3.06×10^{-22}	1.09×10^{-22}	7.8×10^{-23}	5.2×10^{-23}
350	3.80×10^{-22}	9.21×10^{-23}	4.3×10^{-23}	2.0×10^{-23}
351	3.14×10^{-22}	9.48×10^{-23}	6.1×10^{-23}	5.6×10^{-23}
352	2.47×10^{-22}	2.36×10^{-22}	2.13×10^{-22}	2.17×10^{-22}
353	2.44×10^{-22}	1.02×10^{-22}	6.9×10^{-23}	5.2×10^{-23}
354	1.34×10^{-22}	6.73×10^{-23}	1.1×10^{-23}	1.00×10^{-23}
355	1.00×10^{-22}	3.16×10^{-23}	6×10^{-24}	5.0×10^{-24}
356	7.6×10^{-23}	5.26×10^{-23}	2.6×10^{-23}	1.0×10^{-23}
357	1.35×10^{-22}	9.58×10^{-23}	3.2×10^{-23}	9×10^{-24}
358	1.03×10^{-22}	5.34×10^{-23}	6×10^{-24}	$< 10^{-24}$
359	5.4×10^{-23}	2.1×10^{-24}	$< 10^{-24}$	$< 10^{-24}$
360				
361	4.9×10^{-23}	2.1×10^{-24}	$< 10^{-24}$	4×10^{-24}
362	7×10^{-24}	$< 10^{-24}$	$< 10^{-24}$	$< 10^{-24}$
363	3.1×10^{-23}	$< 10^{-24}$	$< 10^{-24}$	$< 10^{-24}$
364	7×10^{-24}	2×10^{-24}	$< 10^{-24}$	$< 10^{-24}$
365	2.2×10^{-23}	9×10^{-24}	$< 10^{-24}$	$< 10^{-24}$
366	3.0×10^{-23}	1×10^{-24}	$< 10^{-24}$	$< 10^{-24}$
367	3×10^{-24}	$< 10^{-24}$	$< 10^{-24}$	$< 10^{-24}$
368	2.1×10^{-23}	9×10^{-24}	$< 10^{-24}$	$< 10^{-24}$
369	1.1×10^{-23}	6×10^{-24}	$< 10^{-24}$	$< 10^{-24}$
370	1.0×10^{-24}	$< 10^{-24}$	$< 10^{-24}$	$< 10^{-24}$

Cross section values in cm^2.

BEST DOCUMENT AVAILABLE

IV QUANTUM YIELD MEASUREMENTS

A. Equipment and Procedures

The quantum yield apparatus is schematically diagrammed in Figure 3.

The light source for these experiments was a Chromatix CMX-IV flash-lamp pumped, frequency doubled, tunable dye laser. The output, which covered the range 265-330 nm, was obtained using Coumarin 522, Sodium Fluorescein, Rhodamine 575, Rhodamine 6G, and Rhodamine 640. The 900-ns-wide pulse emitted between 4×10^{13} (at 265 nm) to 1.0×10^{15} (at 300 nm) photons per pulse. The laser was operated between 5 and 35 pulses per second. Since several hundred to as many as 3000 shots were necessary to generate a signal, the output was constantly monitored during the $O(^1D)$ emission experiments by a Laser Precision Co. Model RK 3232 power meter. The laser beam was monitored after passing through the cell. The power meter was calibrated at 290 nm and 310 nm using a ferrioxalate chemical actinometer. It was found that the detector head had deteriorated so that the absolute power readings were only approximately 71% of the power in the beam as determined from the actinometry. However, the detector sensitivity as a function of wavelength only varied about 4% between these two wavelengths. Further actinometric measurements at 280 and 330 showed a 6% differential over the whole range. These values were used to correct the detector sensitivity as a function of wavelength.

Two reaction cells were used. One, with no outer jacket, was used for some of the room temperature $O(^1D)$ fluorescence determinations. It was found that the jacketed cell, with no provisions for Wood's Horns, actually increased observed $O(^1D)$ fluorescence slightly (presumably some 630-nm photons reflected off the rear wall). When the cell was used for resonance fluorescence measurements, black velvet was used to reduce the scattered light intensity to allow measurements of $O(^3P)$ resonance scattering in the same cell.

The main cell consisted of a 15 cm long by 25 mm diameter Pyrex inner chamber, surrounded by a jacket through which cooled methanol was

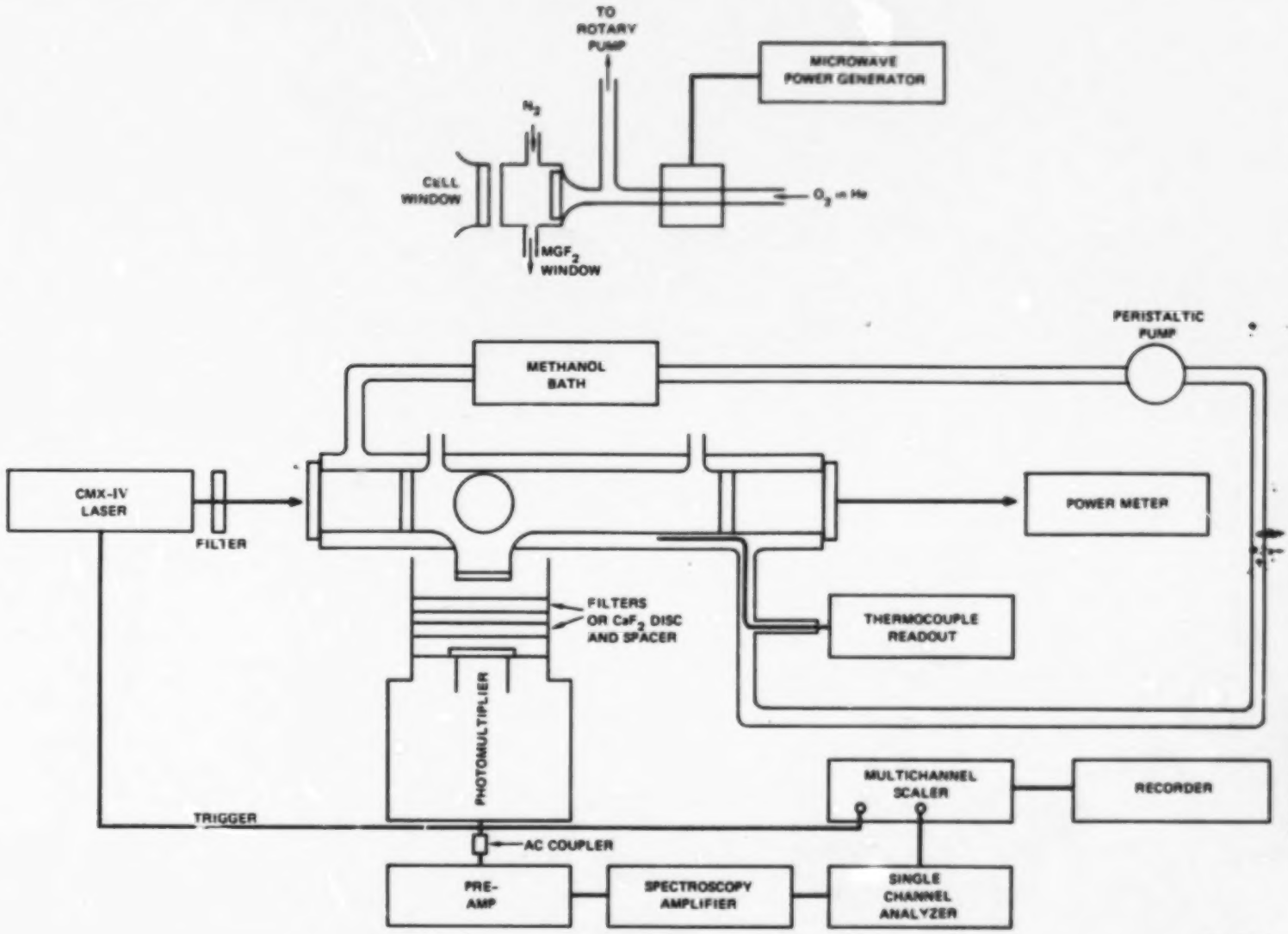

BEST DOCUMENT AVAILABLE

FIGURE 3 APPARATUS USED FOR MAKING QUANTUM YIELD MEASUREMENTS

The distance between the laser and reaction cell was about 3 m to minimize the effects of any electronic noise on the detection system. The photomultiplier was a red-sensitive RCA C31034 for $O(^1D)$ system, while a solar blind EMR 542G P.M. tube was used for the $O(^3P)$ resonance fluorescence system. Black velvet was placed opposite to the lamp and to the P.M. tube to reduce light scattered directly from the lamp.

BEST DOCUMENT AVAILABLE

flowed. Double windows at the ends kept the inner surfaces cool to prevent significant thermal losses, and calcium oxide between the windows prevented fogging due to condensation. The side windows were isolated from atmospheric moisture by direct contact with optical elements of the detection system, or by a small quartz evacuated spacer.

Ozone was prepared as described for the absorption measurements. The pressure measurements were made by means of a Gould model 580-A absolute reading capacitance nanometer.

For the $O(^1D)$ emission measurements, the detection system consisted of a 630-nm interference filter (Optics Technology, $\Delta\lambda$ = 0.26 nm), a UV blocking interference filter, and an RCA C31034 red-sensitized photomultiplier cooled to a dry ice temperature to reduce dark-current pulse rate at 1450 volts. The pulses from the photomultiplier were fed through a preamplifier, amplifier and discriminator before being counted in the Canberra 8000 Multichannel Analyzer (MCA). The MCA had a channel width of 10 μs and a maximum count rate of 5×10^7 cps. It was triggered by the laser trigger gate pulse. The jitter and delay between the lamp firing and the trigger pulse to the MCA were observed to be less than 1 μs.

In a typical $O(^1D)$ emission experiment, ozone would be first mixed with helium in about a 1 to 10^4 ratio and stored temporarily in a 10-liter bulb at about one atmosphere. The mixture would then be slowly flowed through the cell, the laser turned on, and the output sampled as the experiment went on. The total pressure was monitored and kept to within 1% at 0.1 to 8 torr total pressure. The average residence time of an average ozone molecule in the 5-mm beam of the laser was about eighty shots. Much less than .01% of the ozone was photolyzed in each shot, however.

Typically, the procedure for the $O(^3P)$ measurements was the same except that the laser intensity was not monitored. N_2 and H_2 were added in small quantities to the O_3/He mixture in the bulb for some experiments.

Also, for $O(^3P)$, a microwave-discharge resonance lamp of conventional design was made using MgF_2 and CaF_2 optics. An EMI-Photoelectric Co. 542G-09 solar blind photomultiplier with magnesium fluoride windows was

BEST DOCUMENT AVAILABLE

used as the detector. The signal was processed in the same way as in the case of $O(^1D)$.

B. Results

In pure ozone with a helium buffer the $O(^1D)$ and $O(^3P)$ concentrations were governed by:

$$O_3 + h\nu \xrightarrow{\phi^1D} O(^1D) + O_2\ (^1\Delta) \quad (16)$$

$$O_3 + h\nu \longrightarrow O(^1D) + O_2\ (X^3\Sigma) \quad (17)$$

$$O_3 + h\nu \xrightarrow{\phi(^3P)} O(^3P) + O_2 \quad (18)$$

$$O(^1D) + O_3 \xrightarrow[\text{Ref. 41}]{2.5 \times 10^{-10}} O(^3P) + O_3 \quad (19)$$

$$O(^3P) + O_3 \xrightarrow[\text{Ref. 39}]{1.0 \times 10^{-14}} 2O_2 \quad (20)$$

$$O(^1D) \longrightarrow O(^3P) + h\nu \quad (21)$$

Since the field of view for both the emission and resonance fluroescence systems was much larger than the diameter of the photolysis region (5-6 mm diameter laser beam), diffusion and wall reactions were unimportant in the 100-1500 μs time scale used. Thus, in excess ozone the concentration of $O(^1D)$ should be governed by:

$$[O(^1D)] = [O(^1D)]_o\ e^{-k[O_3]t} \quad (22)$$

where $k = 2.5 \times 10^{-10}$ and $[O(^1D)]_o$ is the concentration of $O(^1D)$ immediately after the flash. Since the radiative lifetime of $O(^1D)$ is long compared to the chemical lifetime, the emission signal, in counts per

BEST DOCUMENT AVAILABLE

second, was directly proportional to the [O(^{1}D)] and thus the number of counts in each channel of the MCA (C_n) is given by:

$$C_n = C_1 e^{-k[O_3]n\Delta t} = C_1 e^{-n\Delta t/\tau}$$

where Δt is the channel width, n is the channel number, and τ is the time the signal decays to 1/e of its initial value. τ should be much greater than Δt . The number of counts that should be in the first channel can be obtained by linear regression of a plot of log C_n versus n. It can easily be shown[39] that the initial intensity in counts per second at t=0 is related to the number of counts in the first channel by:

$$I_o = \frac{C_1}{\tau(e^{-\delta/\tau} - e^{-\Delta t/\tau})} \qquad (24)$$

where δ is the dead switching time between channels. (This time is 0.1 μs for the Canberra 8000 used to make these measurements). In practice, δ and Δt were much smaller than τ so that I_o differed from $C_1/\Delta t$ by only a few percent. This is the limit for (24) as δ and Δt approach zero.

The experimental results from the O(^{1}D) emission experiments can be seen (Figure 4) to conform to the expected decay behavior, with a decay time consistent with the rate constant of $(2.7 \pm 1.5) \times 10^{-10}$ cc molec^{-1} sec^{-1}. The zero ozone concentration disappearance rate for O(^{1}D), obtained by linear regression of a rate vs. [O_3] plot, was less than 10^{-1} sec^{-1}; however, evidence for a diffusion or diffusion-like process could be seen in the decay curves at the lowest helium pressure used (1 torr).

The relative primary quantum yield for O(^{1}D) production is given by:

$$(\phi(^1D))_{rel} = \frac{I_o}{\sigma \cdot n \cdot (P_L/\lambda)} \qquad (25)$$

where P_L is the average laser power or total energy after n shots, λ is the wavelength, n is the number of shots, and σ is the absorption cross section of ozone. Values of $\sigma(^1D)_{rel}$ are given in Table 4.

BEST DOCUMENT AVAILABLE

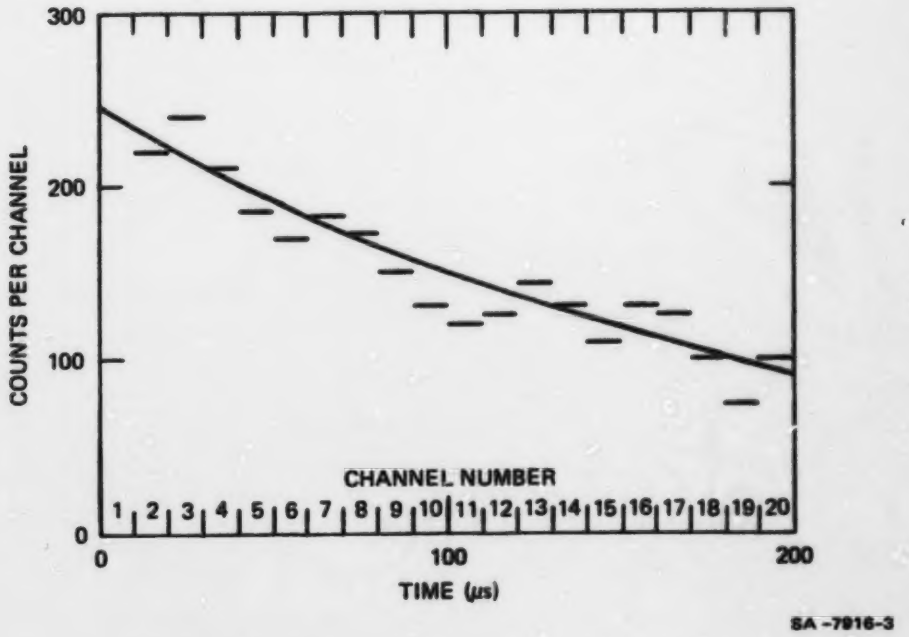

FIGURE 4 TYPICAL O(^{1}D) EMISSION SIGNAL

O(^{1}D) emission results for λ = 305 nm 1000 shots.
$[O_3] = 2.16 \times 10^{13}$ cc^{-1}. Apparent rate constant: 2.8×10^{-10} cc-moles^{-1} sec^{-1}
Initial intensity = 241 $\pm$ 23 counts per 10 μs per 1000 shots.
First channel not used in determination.
Helium Pressure: 9.4 torr. 298 K.

BEST DOCUMENT AVAILABLE

For $O(^3P)$ the situation was a bit more complicated; consequently, fewer measurements were made. Since it has now been clearly demonstrated a number of times (Davenport[39,40] and Weisenfeld[35,37]) that $O(^1D)$ reacts with ozone to produce exactly one $O(^3P)$, and since the rate constant for the production of $O(^3P)$ should be the same as for the disappearance of $O(^1D)$, the $O(^3P)$ should be governed by:

$$[O(^3P)] = [O(^3P)]_o + (1 - e^{-k[O_3]t})[O(^1D)]_o \qquad (26)$$

Equations (22) and (26) describe our system, which is applicable for any O_2 fragment, as long as it does not react quickly with ozone to produce $O(^3P)$ or $O(^1D)$. This is certainly the case for $O_2(^1\Delta)$ (rate constant = 2.5×10^{-15} cm^3 $molec^{-1}$ sec^{-1}) and vibrationally excited O_2 on the time scales used here. However, $O_2(^1\Sigma) + O_3$, with a rate constant one tenth that of $O(^1D) + O_3$, could conceivably affect our results by a factor of two if $O_2(^1\Sigma)$ were produced with unit quantum efficiency. That is, the $O(^1D)_o$ of equation (24) would properly be replaced by $[O(^1D)]_o + [O_2(^1\Sigma)]_o$. However, it has been well established[41] that $O_2(^1\Sigma)$ production in the Hartley band is less than 10%.

The analysis for determining the initial signal intensity is given by equation (24). In the case of $O(^3P)$, however, an absolute quantum yield can be determined. Assuming the decay of the $O(^3P)$ to be negligible (which makes the regression calculations much simpler), the ratio of I_o to the plateau intensity for $O(^3P)$ resonance fluorescence at times long compared to the time constant for $O(^1D) + O_3$, will be the absolute quantum yield assuming $O_2(^1\Sigma)$ does not produce extra $O(^3P)$. This is because all the $O(^1D)$ formed in the initial photolysis is converted to $O(^3P)$ before $O(^3P)$ decay can occur to a significant extent.

The quantum yield values thus obtained are shown in Figure 5. They can be used to put the more extensive $O(^1D)$ emission quantum yields on an absolute basis.

Experiments were conducted with H_2 and with N_2 present as efficient reactant and quencher, respectively, for $O(^1D)$. The H_2 results slowed

BEST DOCUMENT AVAILABLE

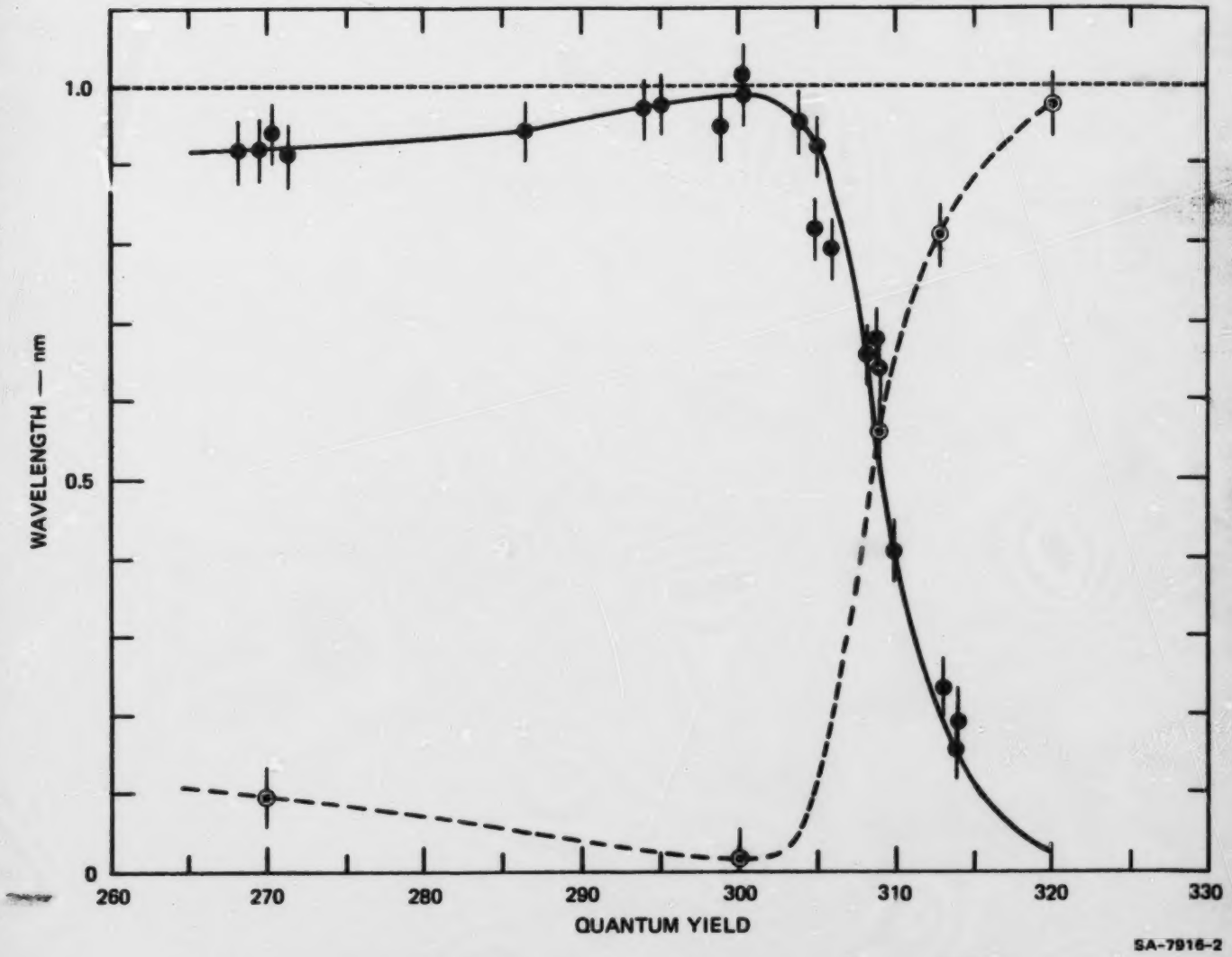

FIGURE 5 ROOM TEMPERATURE VALUES FOR ATOMIC OXYGEN QUANTUM YIELDS

● (^{1}D) values based on measurement of Φ (^{1}D) = 1.00 at 300 nm.
◉ (^{3}P) absolute values.
Lines drawn primarily on basis of Φ (^{3}P) values. Vertical lines represent 90% uncertainty limits in determining the zero time intensity.

BEST DOCUMENT AVAILABLE

the initial formation of $O(^3P)$ so that initial signals could be obtained more precisely; however, secondary reactions that lead to chains did not allow for absolute quantum yield measurements. Instead, the initial intensity derived had to be compared to the maximum intensity in pure ozone or with up to 1.0 torr N_2 present with the ozone. These experiments served primarily to help establish that secondary reactions were not contributing to the $O(^3P)$ signal.

The temperature dependence was obtained for both the $O(^1D)$ and $O(^3P)$ by obtaining the ratios of initial intensities for two runs under identical conditions except that the temperature was changed. Thus relative values were actually obtained and they are given in Table 4. The $O(^1D)$ signal at the lowest temperature used was just discernible at 313 and represents the limit of our sensitivity. In order to obtain the value listed, runs of up to 5,000 shots were taken. The $O(^3P)$ signals were too uncertain to be used to determine the $\phi(^1D)$ value under these conditions.

Experimental running times for all experiments ranged from 15 minutes to 2 hours, with 20-30 minutes being the norm.

Table 4

QUANTUM YIELD RATIOS FOR QUANTUM YIELDS AT
TEMPERATURES GIVEN TO QUANTUM YIELDS AT ROOM TEMPERATURE (300 K)

	270 nm		300 nm		313 nm	
	$\phi(^1D)_T/\phi(^1D)_{300\ K}$	$\phi(^3P)_T/\phi(^3P)_{300}$	$\phi(^1D)_T/\phi(^1D)_{300\ K}$	$\phi(^3P)_T/\phi(^3P)_{300}$	$\phi(^1D)_T/\phi(^1D)_{300\ K}$	$\phi(^3P)_T/\phi(^3P)_{300}$
268 K	1.02 ± .13	1.00 ± .31	.95 ± .13	.93 ± .20	.84 ± .12	1.14 ± .18
198 K	1.10 ± .13	.91 ± .32	1.03 ± .15	1.08 ± .19	0.042 ± .010	1.23 ± .18

Error limits are two standard deviations for the three separate measurements made for each value shown above. Each of the three values used were weighted inversely with respect to the statistical uncertainty in determining the signal as described in the text.

BEST DOCUMENT AVAILABLE

BEST DOCUMENT AVAILABLE

V DISCUSSION

The absolute absorption coefficients at room temperature, given in Table 2, agree well with the data in the literature as shown in Table 5. At lower temperatures, there are only two previous studies, those of Simons et al.[42] who do not calculate their values for 300 and 200 K, and those of Vigroux.[4-11] In general, allowing for interpolation errors for temperature, the Vigroux values for absorption valleys are typically higher than those for Simons et al. at low temperatures. However, the room temperature values[43] for Simons et al. seem higher than those of Inn and Tanaka and Griggs. Our values range to about 5-10% lower than Vigroux's values in the valleys and tend to favor his results over those of Simons et al., though interpolation and extrapolation of the various data could account for most of the differences. There were some definite differences between the absorption spectra of Inn and Tanaka[3] and of Griggs[2] and our spectrum. Specifically, the shoulder in our data at 321.0 nm, shown clearly in Figure 3, is missing in the referenced data.[23] However, it is clearly shown in Simon et al.[42] Our spectra, again in agreement with Simons et al. show the peak to occur at 323.1 nm, not the absorption valley as in the other works. There is a small peak missing in the data of Inn and Tanaka at 326.3 nm which appears in the present work, as well as in Simons et al. and Griggs. Finally, many spectrum features at wavelengths above 346 nm which are present in the present work and in Simons et al., are totally missing from both Grigg's and Inn and Tanaka's work. In general, these are only minor differences in the spectra if they are only to be used to calculate photolysis rates. In particular, there is good agreement in the 250-320 nm region.

At room temperature, the quantum yield data below 300 nm are in agreement with those of Fairchild et al.[34] and Sparks et al.,[36] except that we only see 8% $O(^3P)$ production at 270 nm at room temperature. The 7% value for $O(^3P)$ obtained at 190 K shows that within experimental error, the quantum yield for $O(^3P)$ production changes very little with temperature in the range studied.

BEST DOCUMENT AVAILABLE

Table 5

COMPARISON OF ABSOLUTE ABSORPTION COEFFICIENT MEASUREMENTS

Wavelength (nm)	Reference 12	Reference 2	Reference 17	Present Work[d]
253.7	306.5	303.5	310.8	304.2
296.7	39.4	39.8	39.8	39.5
334.1 nm	0.150	0.150	--	0.149

Values in atm^{-1} cm^{-1} S.T.P., base e.

[12] E.C.Y. Inn and Y. Tanaka, J. Opt. Soc. Amer. 43, 870 (1953).

[2] M. Griggs, J. Chem. Phys. 49, 857 (1968).

[17] W. B. DeMore and O. Raper, J. Phys. Chem. 68, 412 (1964).

[d] From a series of measurements at each wavelength. Absorption coefficient given by $\ln [(I_O - I_B)/(I-I_B)]/\ell P$, where I_B is the background photomultiplier dark current, I_O is the current without ozone present, I is the current after O_3 is added to the cell at temperature corrected pressure $P = (273K/299K)P_O$ where P_O is the observed pressure in atmosphere, and ℓ is the path length, which in this case was 396 ± 0.4 cm.

At 313 nm the temperature dependence data presented in Table 4 seem to agree within experimental error with the data of Kajimoto and Cvetanovic,[26] with Liu and De More.[31] These results show a greater decrease in $O(^1D)$ quantum than those of Kuis et al.[29] Using the empirical arctan expression derived by Moortgat and Kudjus, which fits their data well, we calculate that the expected $O(^1D)$ primary quantum yield values at 313 would be 0.28, 0.18, and .0085 at 300, 270, and 198 K respectively, compared to our experimental values of .19, .15, and .008 respectively. All these values, except the first, at 300°K, are within experimental error at corresponding temperatures. The value of .19 is the value (from Figure 5) from which

BEST DOCUMENT AVAILABLE

the others are derived using the data from Table 4. Thus, our data do not agree with the room temperature value for the quantum yield derived by the equations and, more important, do not show the drop-off with temperature predicted by the formula at 270°K. Thus, even if the value for $\phi(^1D)$ is actually 0.28, our data shows that the quantum yield at 270 would be 0.23.

Using a symmetrical top model we estimated ground state internal energy population distributions to test whether the $O(^1D)$ quantum yield has a wavelength profile consistent with a threshold photodissociation process. In this model, rotational energy is pooled with photon energy to cause the transition to the continuous dissociative state. For an oblate symmetrical top, the energy terms are given by:[44]

$$E_{JK} = BJ(J + 1) + (A - B)K^2$$

where K and J are rotational quantum numbers where K has all integral values between $\pm |J|$. A and B are rotational angular momentum constants which are given by[44] 3.55348 and .420020 cm^{-1} respectively, for ozone. Actually ozone is not quite a symmetrical top molecule and the asymmetrical energy constants are actually given by[44] A = .355348, B = .44525, C = .39479. Thus in making this calculation absolute we assumed that neither .445 or .395 varied significantly from .42.

BEST DOCUMENT AVAILABLE

The centripidal distorcion factors have been ignored since we are dealing with relatively low temperature threshold phenomena. A degeneracy of $2J + 1$ is associated with each energy level with a quantum number J, and each non-zero K level is doubly degenerate. Thus, the relative polulation of each energy level P_{JK} can be given by the Maxwell-Boltzman distribution law:

$$\frac{P_{K,J}}{N} = g_o(2J + 1)\exp(- E_{JK} \cdot \frac{hc}{kT})$$

where $P_{K,J}$ is the population of the rotational energy level with quantum numbers J and K, and where $g_o = g_K \cdot K$, g_K is the nuclear spin statistical weighting factor which equals 1 for K = 0,2,4....and zero otherwise and K is 2 for all $K \neq 0$, 1 otherwise. N is a normalization factor which is equal to the total population in the vibrational ground state divided by the rotational partition function. Relative populations $P_{K,J}/N$ were calculated to energies of 1220 cm^{-1} corresponding to a J quantum number value of 20 and an equivalent wavelength of 320 nm (308 nm is the dissociation energy). This is at the limits of this model since we did not include vibrational influences on the population and because we did not include the centrifugal stretching correction.

By performing these calculations, we found that the difference between the calculated and measured percentage reduction in quantum yields with temperature at given wavelengths is within our experimental error. However, the $P_{K,J}/N$ value at 313 and room temperature is about 8% lower than found experimentally.

Experimental quantum yield values marginally higher than expected from these sample calculations have also been reported by Brock and Watson[47] in the case of ozone, and by Davenport[48] and others in the case of NO_2. For ozone however, recent calculations by Hudson[45] using a large computer with none of the simplifying assumptions used above has succeeded in matching the data of Watson et al.[47] very closely without having to invoke a third photolytic process, such as for instance production of $O_2(^1\Sigma) + O(^3P)$.

BEST DOCUMENT AVAILABLE

BEST DOCUMENT AVAILABLE

It was not the purpose of this work, however, to totally elucidate the detailed mechanism by which O_3 photolyzes. The data are not extensive enough to do this. They were obtained primarily to provide an accurate basis upon which to calculate stratospheric O_3 primarily photolysis rates and $O(^1D)$ and $O(^3P)$ moderation rates. Combination of the values of σ and $\phi(^1D)$ given in this report with known photon fluxes, ozone concentration, and atmospheric temperatures should yield values for $O(^1D)$ production rates that are accurate to within 10% at room temperature, or about 25% at about 200 K, plus the percent error in the flux values.

BEST DOCUMENT AVAILABLE

BEST DOCUMENT AVAILABLE

VI REFERENCES

1. H. S. Johnston, "CIAP Monograph I," The Natural Stratosphere of 1973, A. J. Grosbecker, Ed., Final Report DOT-TSC-74-51, National Technical Information Service, Springfield, Virginia (September 1970), pp. 5-17 to 5-35.

2. M. Griggs, J. Chem. Phys. 49, 957 (1968).

3. E.C.Y. Inn and Y. Tanaka, in Ozone Chemistry and Technology, Advanced in Chemistry Series, No. 21, American Chemical Society Applied Publications, (1959), p. 263.

4. E. Vigroux, Ann. Phys. (Series 6) 8, 709 (1953).

5. E. Vigroux, C. R. Acad. Sci. Paris 230, 2170-2 (1950).

6. E. Vigroux, C. R. Acad. Sci. Paris 230, 2277-8 (1950).

7. E. Vigroux, C. R. Acad. Sci. Paris 234, 2351 (1952).

8. E. Vigroux, C. R. Acad. Sci. Paris 234, 2439 (1952).

9. E. Vigroux, C. R. Acad. Sci. Paris 234, 2592 (1952).

10. E. Vigroux, C. R. Acad. Sci. Paris 235, 149 (1952).

11. E. Vigroux, Ann, Phys. (Paris), 8, 709-62 (1953).

12. Y. Tanaka and E.C.Y. Inn, J. Opt. Soc. Amer. 43, 870 (1953).

13. E. Vigroux, Ann. Geophys. 25, 169 (1969).

14. E. Castellano and H. Schumacher, Chem. Phys. Letters 13, 625 (1972).

15. I. Jones, U. Kacjmar, and R. Wayne, Proc. Soc. (London) A 316, 431 (1970).

16. H. Taube, Trans. Faraday Soc. 53, 656 (1957).

17. W. DeMore and O. Raper, J. Chem. Phys. 68, 412 (1964).

18. V. Berretta and H. Schumacher, Z. Phys. Chem. B 17, 417 (1932).

19. E. Castellano and H. Schumacher, Z. Physik. Chem. Neue Folge 65, 62 (1969).

BEST DOCUMENT AVAILABLE

20. E. Castellano and H. Schumacher, Z. Physik Chem. Neue Folge 76, 258 (1971).

21. I.T.N. Jones and R. P. Wayne, J. Chem. Phys. 51, 3617 (1969).

22. R. Simonaitis, S. Broslovsky, J. Heicklen, and M. Nicolet, Chem. Phys. Letters 19, 601 (1973).

23. M. Gauthur and D. Snelling, J. Chem. Phys. 54, 4317 (1971).

24. G. von Ellenreider, E. Castellano, and H. Schumacher, Z. Physik. Chem. Neue Folge 76, 240 (1972).

25. E. Lissi and J. Heicklen, J. Photochem. 1, 39 (1972/73).

26. O. Kajimoto and R. J. Cvetanovic, Chem. Phys. Lett. 37, 533 (1967).

27. D. Martin, G. Girman, and H. S. Johnston, 167th ACS National Meeting, Los Angeles, California (1974).

28. G. Moortgatt and P. Warneck, Z. Naturforsch. A 30, 835 (1975).

29. S. Kuis, R. Simonaitis, and J. Heicklen, J. Geophys. Res. 80, 1328 (1975).

30. I.T.N. Jones and R. P. Wayne, Proc. Roy. Soc. A 319, 273 (1970).

31. C. Lin and W. B. DeMore, J. Photochem. 2, 161 (1973/74).

32. P. Philen, R. Watson, and D. Davis, J. Chem. Phys. 67, 3316 (1977).

33. I. Arnold, F. J. Comes and G. K. Moortgatt, Chem. Phys. 24, 211 (1977).

34. C. E. Fairchild, E. J. Stone, G. M. Lawrence, J. Chem. Phys. 69, 3632 (1978).

35. J. Wiesenfeld, Informal Conference on Photochemistry (1980).

36. R. Sparks, L. Carlson, K. Shobatake, M. Kowalczyk, and Y. Lee, J. Chem. Phys. 72, 1401 (1980).

37. S. T. Amimoto, A. P. Force, and J. R. Wiesenfeld, Chem. Phys. Lett. 60, 40 (1978).

38. P. W. Fairchild and E.K.C. Lee, Chem. Phys. Lett. 60, 36 (1978).

39. J. E. Davenport, Ph.D. dissertation, "The UV Photolysis of Ozone," York University, Toronto, Canada (1973).

BEST DOCUMENT AVAILABLE

40. J. E. Davenport, B. Ridley, H. I. Schiff, and K. H. Welge, Disc. Faraday Soc. 53, 230 (1972).

41. R. Gilpin, H. Schiff, and K. Welge, J. Chem. Phys. 55, 1987 (1971).

42. J. Simons, R. Paur, H. Webster III, and E. Bair, J. Chem. Phys. 59 1203 (1973).

43. CIAP Monograph 1, "The Natural Stratosphere of 1973," A. J. Grosbecker, Ed., Final Report DOT-TSC-24-51, NTIS, Springfield Va. (1970) p. 5-168.

44. G. Herzberg, Molecular Spectra and Molecular Structure, Volume III, Von Nostrand Reinhold, New York, 1966. pp. 92-93, 222-244, 604.

45. NASA Gooddard Space Flight Center, Greenbelt, Maryland. Hudsen, R. D., private conversations, January and May, 1980.

46. G. K. Moortgat and E. Kudjers, Geophys. Res. Lett., 5, 191 (1978).

47. J. Brock and R. T. Watson, Chem. Phys. 46, 477 (1980).

48. J. E. Davenport, Final Report: "Determination of NO_2 Photolysis Parameters for Stratospheric Modeling." Report No. FAA-EQ-78-14, NTIS, Springfield, Maryland 22161 (1978).